Assessing seasonal and interannual changes in carbonate chemistry across two time-series sites in the North Western Mediterranean Sea

Cathy Wimart-Rousseau, Thibaut Wagener, Anthony Bosse, Patrick Raimbault, Laurent Coppola, Marine Fourrier, Caroline Ulses, Dominique Lefèvre

frontiers | Frontiers in Marine Science

TYPE Original Research
PUBLISHED 23 November 2023
DOI 10.3389/fmars.2023.1281003

OPEN ACCESS

EDITED BY
Xianghui Guo,
Xiamen University, China

REVIEWED BY
Eva Krasakopoulou,
University of the Aegean, Greece
Arthur Capet,
Royal Belgian Institute of Natural Sciences, Belgium

*CORRESPONDENCE
Cathy Wimart-Rousseau
cwimart-rousseau@geomar.de

†PRESENT ADDRESS
Cathy Wimart-Rousseau,
Research Center for Marine Geosciences (GEOMAR) Helmholtz Centre for Ocean Research Kiel, Kiel, Germany

RECEIVED 21 August 2023
ACCEPTED 30 October 2023
PUBLISHED 23 November 2023

CITATION
Wimart-Rousseau C, Wagener T, Bosse A, Raimbault P, Coppola L, Fourrier M, Ulses C and Lefèvre D (2023) Assessing seasonal and interannual changes in carbonate chemistry across two time-series sites in the North Western Mediterranean Sea.
Front. Mar. Sci. 10:1281003.
doi: 10.3389/fmars.2023.1281003

Assessing seasonal and interannual changes in carbonate chemistry across two time-series sites in the North Western Mediterranean Sea

Cathy Wimart-Rousseau[1*†], Thibaut Wagener[1], Anthony Bosse[1], Patrick Raimbault[1], Laurent Coppola[2,3], Marine Fourrier[2], Caroline Ulses[4] and Dominique Lefèvre[1]

[1]Aix Marseille Université, Université de Toulon, Centre national de la recherche scientifique (CNRS), Institut de Recherche pour le Développement (IRD), Mediterranean Institute of Oceanography (MIO), Unité Mixte (UM110), Marseille, France, [2]Sorbonne Université, CNRS, Laboratoire d'Océanographie de Villefranche, Laboratoire d'Océanographie de Villefranche (LOV), Villefranche-sur-Mer, France, [3]Sorbonne Université, CNRS, Observatoire des Sciences de l'Univers (OSU) Station Marines, STAMAR, Paris, France, [4]Laboratoire d'Etudes en Géophysique et Océanographie Spatiales (LEGOS), Université de Toulouse, Centre National d'Etudes spatiales (CNES), CNRS, Institut de Recherche pour le Développement (IRD), Université Toulouse III - Paul Sabatier, Toulouse, France

Sustained time-series measurements are crucial to understand changes in oceanic carbonate chemistry. In the North Western Mediterranean Sea, the temporal evolution of the carbonate system is here investigated based on two 10-year time-series (between January 2010 and December 2019) of monthly carbonate parameters measurements at two sampling sites in the Ligurian Sea (ANTARES and DYFAMED). At seasonal timescale, the seawater partial pressure of CO_2 (pCO_2) within the mixed layer is mostly driven by temperature at both sites, and biological processes as stated by the observed relationships between total inorganic carbon (C_T), nitrate and temperature. This study suggests also that mixing and water masses advection could play a role in modulating the C_T content. At decadal timescale, significant changes in ocean chemistry are observed with increasing trends in C_T (+3.2 ± 0.9 $\mu mol.kg^{-1}.a^{-1}$ – ANTARES; +1.6 ± 0.8 $\mu mol.kg^{-1}.a^{-1}$ – DYFAMED), associated with increasing pCO_2 trends and decreasing trends in pH. The magnitude of the increasing trend in C_T at DYFAMED is consistent with the increase in atmospheric pCO_2 and the anthropogenic carbon transport of water originating from the Atlantic Ocean, while the higher trends observed at the ANTARES site could be related to the hydrological variability induced by the variability of the Northern Current.

KEYWORDS

carbonate system, Mediterranean Sea, North Western Mediterranean Sea, temporal trends, inorganic carbon, seasonal variability

1 Introduction

The ocean plays a critical role in mitigating climate change induced by human activities through CO_2 exchanges at the air-sea interface and sequestration into deep waters [IPCC, 2021]. Annually, the ocean absorbs between *ca.* 25% and 30% of CO_2 emissions by anthropogenic activities [Friedlingstein et al., 2022; Gruber et al., 2023]. Ocean CO_2 uptake induces an increase in hydronium ion concentration [*i.e.*, a decrease in oceanic pH commonly named "ocean acidification"; Doney et al. (2009)] which represents a significant threat to marine organisms [Kroeker et al., 2013] and is likely to affect marine ecosystems [Feely et al., 2004]. Improving our understanding by quantifying oceanic CO_2 uptake, but also predicting scenarios to design adaptation strategies, requires sustained long-term observations of the carbonate system. To achieve these goals, sustained time-series measurements have been established in the framework of international programs [*e.g.*, World Ocean Circulation Experiment (WOCE) and Joint Global Ocean Flux Study (JGOFS); Tanhua et al., 2015]. Based on long-term time-series analyses, positive trends in dissolved inorganic carbon (C_T) and seawater partial pressure of CO_2 (pCO_2) and negative trends in pH have been assessed over the global ocean [Bates et al., 2014; Lauvset et al., 2015].

More reactive to forcing induced by climate change than other oceanic areas [Durrieu de Madron et al., 2011], the Mediterranean Sea is a semi-enclosed marginal sea with warm and highly alkaline waters prone to absorb CO_2 from the atmosphere and transport it to the interior by an active overturning circulation [Schneider et al., 2010; Lee et al., 2011; Álvarez et al., 2014]. As a consequence, several studies have reported a marked decline in the pH of the Mediterranean Sea over the last few decades [*e.g.*, Touratier and Goyet, 2011; Hassoun et al., 2015; Palmiéri et al., 2015; Touratier et al., 2016; Flecha et al., 2019]. Furthermore, the North Western (NW) Mediterranean Sea is one of the few oceanic basins of the world to permit open ocean deep convection [Marshall and Schott, 1999] as a result of intense atmospheric forcing and oceanic preconditioning. From 2010 to 2013, intense deep convection occurred with the maximum mixed layer depth reaching the seafloor every winter at about 2500 m in the Gulf of Lion (GoL) area [Houpert et al., 2016; Testor et al., 2018; Bosse et al., 2021]. In winter 2018, hydrological observations highlighted convection down to at least 1800 m depth in the GoL [Margirier et al., 2020; Fourrier et al., 2022]. In the Ligurian Sea, intermediate mixing events have been observed between 2010 and 2018, with a maximum depth reached by winter convection of 1000 m reported in 2012 and 2013 [Margirier et al., 2020]. Due to bottom-reaching convection, fresh and cold surface waters are mixed with the intermediate and deep waters, and these vertical turbulent exchanges bring nutrients to the surface, oxygen in deep and intermediate levels, and fuel phytoplanktonic growth [Coppola et al., 2017; Mayot et al., 2017; Leblanc et al., 2018]. All those physical and biological processes affect the carbonate chemistry of the area by modifying both the total alkalinity (A_T) and C_T contents. Mixing events bring up to the surface C_T-enriched deep waters while photosynthesis processes induce a resulting C_T drawdown and an A_T increase. Remineralisation of particulate organic matter will have the reverse effects on C_T and A_T. By impacting the CO_2 solubility, temperature variations modify air-sea CO_2 exchanges and the C_T concentration without impacting A_T as the charge balance is not affected [Zeebe and Wolf-Gladrow, 2001].

In the NW Mediterranean Sea, in the framework of the JGOFS-France Program, the DYFAMED (Dynamique des Flux Atmosphériques en MEDiterranée) time-series has been initiated in 1991 to monitor the evolution of the physical and biogeochemical properties in the Ligurian Sea [Marty et al., 2002; Coppola et al., 2021]. The DYFAMED site is isolated from lateral advection of the Northern Current (NC) and is impacted by fresh surface Atlantic Water (AW) and Levantine Intermediate Water (LIW) [Millot, 1999]. The NC results from the merging in the Ligurian Sea of two currents flowing northward on both sides of Corsica (Figure 1). Reinforced by the wind stress along its pathway [Herbaut et al., 1997], it flows along the continental slope mostly in geostrophic balance forcing a cyclonic circulation. The NC is marked by seasonal variability [Albérola et al., 1995; Birol et al., 2010; Prieur et al., 2020] and baroclinic instabilities [Crépon et al., 1982; Millot, 1991]. The DYFAMED site is then surrounded by the NC characterized by a strong horizontal density gradient [Niewiadomska et al., 2008] that hampers lateral inputs [Andersen and Prieur, 2000].

Following the DYFAMED initiative, the ANTARES (Astronomy with a Neutrino Telescope and Abyss environmental RESearch) time-series was initiated in 2009 [Lefèvre, 2010]. While being outside the deep convection area occurring in the GoL, the ANTARES site is located in a key zone for the NC dynamics at the entrance of the GoL shelf [Petrenko, 2003]. Moreover, numerous studies have reported the presence of submesoscale eddies in the NW Mediterranean Sea that can advect newly formed deep waters away from the Dense Water Formation (DWF) area [Bosse et al., 2016; Damien et al., 2017] and interact with the NC [Testor and Gascard, 2006]. The ANTARES and DYFAMED time-series are part of the French MOOSE program (Mediterranean Ocean Observing System for the Environment; https://www.moose-network.fr – Coppola et al. (2019)) that coordinate and maintain fixed long-term observations across Europe.

Based on data acquired in the Ligurian Sea, several studies have shown the control of temperature, biology, and currents on the seasonality of the seawater pCO_2 [*e.g.*, Hood and Merlivat, 2001; Copin-Montégut et al., 2004; D'Ortenzio et al., 2008]. Merlivat et al. (2018) assessed that temperature and C_T have the strongest influence on seawater pCO_2 variability. The NW Mediterranean Sea experiences well-defined spring blooms leading to nutrient depletion [D'Ortenzio and Ribera d'Alcalà, 2009]. Nutrients replenishment occurs seasonally with winter-time deep convection and allows the occurrence of intense biological processes [*e.g.*, Bégovic and Copin-Montégut, 2002; Marty et al., 2002]. *In situ* measurements of air-sea CO_2 fluxes highlighted a gradual change of the area from a source to a sink between summertime and wintertime, respectively [Bégovic and Copin-Montégut, 2002; Copin-Montégut et al., 2004; Louanchi et al., 2009]. Moreover, a recent synthesis of the carbonate system data recorded in the Ligurian Sea between 1998 and 2016 reported both

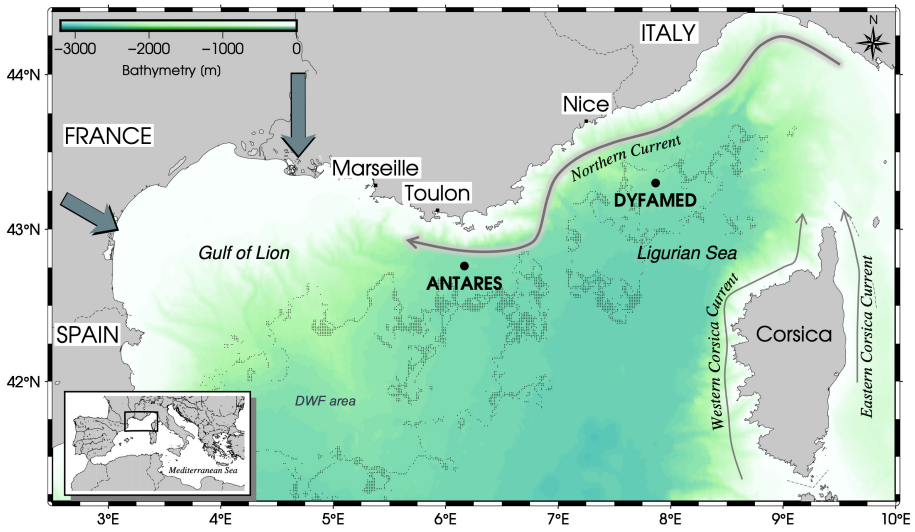

FIGURE 1
Map of the sampling sites ANTARES (42°48'N – 06°05'E) and DYFAMED (43°25'N – 07°52'E) in the North Western Mediterranean Sea. The blue arrows indicate the two dominant wind systems blowing in this area. The main oceanic currents are represented by grey arrows: the Northern Current, the Western Corsica Current and the Eastern Corsica Current. A label in the Gulf of Lion indicates the Dense Water Formation (DWF) site during the 2013 event. The dotted line represents the 0.15 mg m^{-3} contour of surface chlorophyll-a from 8-day merged satellite image (GlobColour project) on 18 February 2013, following Houpert et al. (2016).

clear seasonal cycles and temporal trends for sub-surface waters [Coppola et al., 2020]. In this area, positive trends in C_T (0.59 ± 0.34 µmol kg^{-1} a^{-1}), A_T (0.50 ± 0.21 µmol kg^{-1} a^{-1}) and pCO_2 (3.3 ± 0.7 µatm a^{-1}) and a negative trend in pH (-0.003 ± 0.001 unit a^{-1}) have been assessed over the 18-year period.

This study presents ten years of carbonate chemistry data collected between January 2010 and December 2019 in the NW Mediterranean Sea, at the ANTARES and DYFAMED sites, with the aim of highlighting the main drivers of the temporal variability of the carbonate system at each site. In this paper, these two time-series sites, located *ca*. 150 km apart but in distinct hydrological conditions with respect to NC dynamics, are used to identify the main drivers of carbon variability. With a focus on the carbonate data within the mixed layer, this work: (1) describes the dataset and the specificity of each site, (2) evaluates the drivers of the seasonal carbonate chemistry variability and, (3) estimates and identifies the main drivers of carbonate chemistry changes at longer timescales. By analyzing two time-series from the same oceanic basin as well as by distinguishing trends in offshore and coastal influenced waters, this dual-site approach offers novel perspectives that cannot be gained from analyzing a single site alone and raises novel questions concerning fixed station locations to decipher trends.

2 Material and methods

2.1 Sampling sites

The MOOSE-ANTARES observatory site (named ANTARES hereafter) is located 40 km off the French Mediterranean coast (42° 48'N, 06°05'E) where the water depth is 2475 m (Figure 1). The MOOSE-DYFAMED (named DYFAMED hereafter) observatory site is located *ca*. 50 km off Cape Ferrat in the central zone of the Ligurian Sea and has a depth of 2350 m (43°25'N, 07°52'E).

2.2 Measurements

Measurements are carried out monthly from a research vessel at the DYFAMED and ANTARES sites in the NW Mediterranean Sea (Figure 1). A CTD rosette is deployed with 12 Niskin bottles in order (1) to acquire data with sensors (Conductivity Temperature and Depth - CTD and associated parameters) along vertical profiles, and (2) to collect discrete seawater samples for chemical analysis. A detailed description of the sampling methodology and the CTD sensors can be found in Coppola et al. (2018) for the DYFAMED site. The same procedure is applied at ANTARES. Samples for C_T and A_T were collected into acid-washed 500 cm^3 borosilicate glass bottles, poisoned with 200 mm^3 of a 36 $g.dm^{-3}$ $HgCl_2$, as recommended by Dickson et al. (2007) and stored in the dark at 4°C. Analyses were performed after a few months of storage (less than 6 months). Measurements of C_T and A_T were performed simultaneously by potentiometric acid titration using a closed cell following the methods described by Edmond (1970) and Dickson and Goyet (1994). Analyses were performed at the National Facility for Analysis of Carbonate System Parameters (SNAPO-CO2, LOCEAN, Sorbonne University – CNRS, France) with a prototype developed there. The average accuracy of A_T and C_T analysis estimated from repeated measurements of Certified Reference Material (provided by Prof. Dickson's laboratory from the Scripps Institution of Oceanography, San Diego) is between ± 2 and 5 µmol.kg^{-1}, respectively. Samples for dissolved inorganic nutrients were collected and analysed following the protocol of Aminot and Kérouel (2007). Over these ten years of sampling, 44

and 60 samples for carbonate chemistry measurements have been obtained at ANTARES and DYFAMED, respectively.

2.3 Derived data

2.3.1 Estimation of the mixed layer depth

The Mixed Layer Depth (MLD) was computed using a potential density threshold of 0.03 $kg.m^{-3}$ with a reference depth of 10 dbar [D'Ortenzio et al., 2005]. Vertical profiles of temperature and salinity from the CTD were used to estimate the density. When no value was available at 10 dbar, the shallowest value available above 20 dbar was used. For the MLD determination, only CTD downcast performed when samples were taken have been used in this study.

2.3.2 Carbonate system derived parameters

Seawater carbonate system parameters were derived from A_T and C_T values with the software program CO2SYS-MATLAB [van Heuven et al., 2011] using temperature, salinity, pressure, silicate and phosphate concentrations. As recommended for the Mediterranean Sea by Álvarez et al. (2014), the carbonic acid dissociation constants K_1 and K_2 from Mehrbach et al. (1973) as refitted by Dickson and Millero (1987) and the dissociation constant for HSO_4^- from Dickson (1990) were used. Uppström (1974) was used to calculate the ratio of total boron to salinity and Dickson and Riley (1979) to calculate the hydrogen fluoride constant K_F. To remove the impact of salinity variations (evaporation/precipitation) on A_T and C_T values, salinity-normalised A_T (NA_T) and C_T (NC_T) were calculated by dividing by *in situ* salinity and multiplying by a constant salinity set at 38 following previous studies conducted in the Mediterranean Sea [Bensoussan and Gattuso, 2007; Rivaro et al., 2010; Kapsenberg et al., 2017].

2.3.3 Variability of the seawater pCO_2

The effects of non-thermal (pCO_2^N) and thermal (pCO_2^{TD}) processes on seawater pCO_2 variations have been calculated thereafter following Equations 4.1 and 4.2 [Takahashi et al., 1993; Takahashi et al., 2002]:

$$pCO_2^N = pCO_2^{IS} \times \exp\left(0.0423\left(T_{mean} - T_{obs}\right)\right) \quad (1)$$

$$pCO_2^{TD} = pCO_2^{mean} \times \exp\left(0.0423\left(T_{obs} - T_{mean}\right)\right) \quad (2)$$

where pCO_2^{IS} is the seawater pCO_2 calculated at *in situ* temperature (in µatm), pCO_2^{mean} is the mean seawater pCO_2 over the study period in the mixed layer (397 µatm and 386 µatm at ANTARES and DYFAMED, respectively), T_{mean} is the average mixed layer temperature (in °C, equals to 18.52°C and 16.79°C at ANTARES and DYFAMED, respectively) and T_{obs} is the *in situ* temperature (in °C). pCO_2^N represents a temperature-normalised seawater pCO_2, and pCO_2^{TD} represents the seawater pCO_2 induced by temperature fluctuations under isochemical conditions.

2.3.4 Estimations of CO_2 exchanges

To address the question of the "source" ($pCO_2^{IS} > pCO_2^{ATM}$) or "sink" ($pCO_2^{IS} < pCO_2^{ATM}$) status of both sites for atmospheric CO_2, and their temporal evolution, the pCO_2 excess (ΔpCO_2 in µatm) was calculated as:

$$\Delta pCO_2 = pCO_2^{IS} - pCO_2^{ATM} \quad (3)$$

where pCO_2^{ATM} is the atmospheric partial pressure of CO_2 recorded at the Lampedusa site from January 2010 to December 2019 [Dlugokencky et al., 2021]. Molar fractions of atmospheric CO_2 (xCO_2^{ATM}) were converted into pCO_2^{ATM} using the same atmospheric pressure but the monthly temperature and salinity values measured at each site.

2.4 Estimation of deseasonalised data

In the NW Mediterranean Sea, numerous studies [*e.g.*, Bégovic and Copin-Montégut, 2002; Marty and Chiaverini, 2010] have reported seasonal cycles of the biogeochemical parameters over the year in the upper water column. Following a regular pattern, these seasonal cycles were represented in this study by a harmonic function for each parameter as detailed in Gruber et al. (1998):

$$Param_{fit} = Param_{mean} + a \times sin(2 \times \pi \times d/365) + b \times cos\,(2 \times \pi \times d/365) \quad (4)$$

where $Param_{mean}$ is the mean of the parameter values in the mixed layer over the 10-year period, d is the day of the year, and a and b are fitting coefficients obtained by a nonlinear least squares regression between the data and the harmonic model. The obtained parameters, specific to each variable, including their significance (p-value) are given in Table 1 of the Supplementary Material. In addition, to test the significance of the harmonic fit, the significance of the linear regression between the measured data and the fit function was tested by means of the Pearson coefficient for parametric tests [Sokal and Rohlf, 1969] with a significance level of 95%.

Using a bootstrap method [Zoubir and Iskander, 2007], random fitting parameters have been obtained. The edges of this bootstrap method were defined by the asymptomatic parameters obtained with a covariance matrix. When considering all the quantiles calculated for each simulation, the confidence interval associated with each temporal trend encompassed the variability associated with the fitting parameters perturbation. Thus, the identified interannual trends are not affected by assumptions taken for the deseasonnalisation methodology.

2.5 Detection of the Northern Current position

The near-surface salinity (50-100 m average) was compared to a climatology of the NC deduced from repeated measurements by autonomous gliders [Testor et al., 2019] carried out along endurance lines of the MOOSE program. A total of 113 and 27 glider sections of the NC linking the coast to the DYAMED and ANTARES sampling sites were performed from 2007 to 2013 [Testor et al., 2017]. They were used to build a mean section of salinity according to the distance to the location of the NC peak

velocity. Gliders can be used to infer absolute geostrophic velocities for each NC section by integrating the thermal wind balance combined with depth-average currents [Bosse et al., 2021]. Depth-average currents are also used to compute cross-front velocities in a local streamwise coordinate system [Todd et al., 2016; Bosse and Fer, 2019].

Composite sections of salinity were constructed by averaging individual sections in a cross-front axis centered at the velocity maximum (Vmax) and normalised by the current width (W) corresponding to the standard deviation, or half-width, of a Gaussian fit of the upper 50 m velocities, as in Bosse and Fer (2019). By doing so, the frontal region of the NC can be defined between -1 and 1 (± W) where most of the density gradient between the coastal and offshore waters occurs. The composite salinity section was then used to infer for each profile at DYFAMED and ANTARES whether the 50-100m average salinity was representative of coastal (<-W), frontal, or offshore (>W) conditions.

3 Descriptive seasonal variability within the mixed layer at the two studied sites

3.1 Hydrological characteristics

The hydrographic conditions encountered at the DYFAMED and ANTARES sites from January 2010 to December 2019 are presented in Figure 2. The depth of the mixed layer shows seasonal variations with successive periods of summer stratification followed by winter mixing at both sites (Figures 2A, F). As only CTD downcast performed when samples were taken have been used in this study to derive the MLD, extreme climatic events with bottom-reaching convection reported from 2010 to 2013 and in 2018 in the GoL are not so clearly visible at the two studied sites located outside of the DWF area (see Figure 1 of the Supplementary Material and Section 1). By using Argo float data, Fourrier et al. (2022) reported MLD increases to around 2000 m in the winter 2012-2013 and in 2018. Interannual variabilities of temperature and salinity within the mixed layer are presented in Figures 2B, C, G, H. Marked seasonal changes were present at both sites with an increase in temperature from April to September, and a decrease from October to March. When compared to the DYFAMED data recorded between 1995 and 2007 [Marty and Chiaverini, 2010] in the upper water column, the summer and winter temperatures in the last decade are warmer than the reference situation of 1995 (blue line on Figure 2B). No significant seasonal cycles have been detected for salinity over the studied period, even if higher salinity values were measured in summer (Figures 2C, H). While almost all salinity values at DYFAMED are above 38, many salinity values below 38 are observed at ANTARES, in response to the presence of surface waters transported by the NC [Van Haren et al., 2011; Berta et al., 2018].

The NC shows seasonal variability in its transport [Albérola et al., 1995] and position [Bourg and Molcard, 2021]. Based on the mean salinity distribution against a normalised distance to NC center (Figures 3A, B), each sampling at ANTARES and DYFAMED could be described according to its distance to the NC center (Figures 3C, D). This classification resulted in contrasted distribution between the two sites. Profiles at DYFAMED are clearly associated with offshore conditions in 78% of cases (83/106) and characterised by higher salinities (mean 50-100 m salinity of 38.37 ± 0.09). To the contrary, ANTARES is almost always in the frontal region characterised by important temperature and salinity gradients. On average, the upper layer salinities are lower but more variable (38.26 ± 0.17) at ANTARES (Figures 3C, D). As a consequence, the ANTARES time-series measurements are influenced by the variability in the location of the NC as they are mostly sampled in the core of the NC or its offshore. At both sites, the measurements are only detected once in the coastal area. This confirms that the two sites are located in contrasting regions with respect to the general circulation.

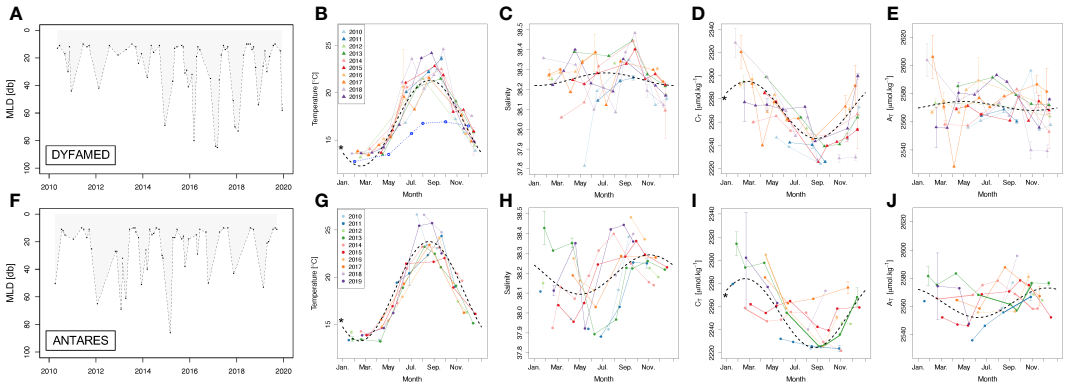

FIGURE 2
(A, F) Temporal variations of the mixed layer depth (MLD) from January 2010 to December 2019 at DYFAMED **(A)** and ANTARES **(F)**. Interannual variability of temperature **(B, G)**, salinity **(C, G)**, total inorganic carbon [C_T – **(D, I)**, total alkalinity [A_T – **(E, J)**] at DYFAMED (upper panel), ANTARES (lower panel). The colour code represents the year and is similar on panels **(B-E, G-J)**. Average values with error bars showing the standard deviation of the mean values have been plotted when multiple data were recorded for the same date within the mixed layer. Dashed lines on panels **(B-E, G-J)** represent the harmonic fit for each parameter. Curves with a star are those where the fitting parameters **(A, B)** are significant. When no data have been acquired during three consecutive months, dots have not been joined. On **(B)**, the blue line indicates mean temperature values over the first 40 meters depth during the reference situation of 1995.

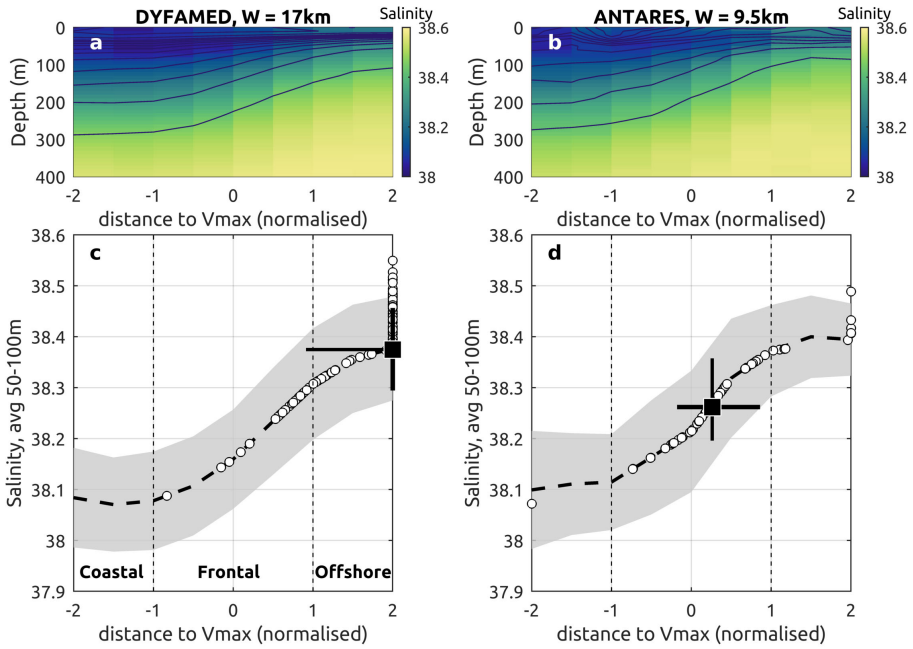

FIGURE 3
Mean section of practical salinity across the Northern Current in normalised cross-front distance from coastal to offshore area at DYFAMED **(A)** and ANTARES **(B)**. The black lines represent isolines of potential density. The NC location is estimated from the steepest isopycnal slope. Practical salinity averaged between 50 and 100 m (mean and standard deviation) at DYFAMED **(C)** and ANTARES **(D)**. The black bar is drawn between the 20th and 80th percentile. The black square is drawn at the median distance and mean salinity. Vmax stands for velocity maximum and W for the width of the current.

3.2 Characteristics of the carbonate system

Temporal variations of the carbonate system parameters over the 10-year period within the mixed layer are described in Figures 2D, E, I, J with interannual changes of C_T and A_T at the DYFAMED (Figures 2D, E) and ANTARES (Figures 2I, J) sites, respectively. Over the period, the mean C_T concentration was slightly higher at DYFAMED (2269 ± 27 µmol.kg^{-1}) than ANTARES (2257 ± 27 µmol.kg^{-1}). A high seasonal variability is visible at both sites, with the highest C_T values measured in autumn and winter and a C_T depletion occurring in spring and summer. In consequence, the seasonal changes in C_T are well represented by the harmonic function. Mean A_T values were almost similar at both sites over the period studied (Table 1). Nonetheless, the amplitude of A_T variations was lower at ANTARES (2536-2596 µmol.kg^{-1}) than at DYFAMED (2528-2626 µmol.kg^{-1}). It has been previously stated that, when biological activity is excluded, the variations in A_T should directly be related to salinity change when dilution or evaporation occurs in the ocean [Copin-Montégut, 1993]. Nonetheless, due to the lack of seasonality of salinity (Figures 2C, H), no clear seasonal signal can be seen for A_T at either site (Figures 2E, J).

3.3 Nutrients

Variations in inorganic nutrients within the mixed layer over the studied period are described in Figures 2A-H of the Supplementary Material. Nutrient concentrations displayed seasonal patterns, with the highest values measured in winter (January-March) and the lowest in late spring or summer. Lower ranges of nutrients concentrations in the MLD were measured at DYFAMED than at ANTARES (Table 1). In the Ligurian Sea, Pasqueron de Fommervault et al. (2015) described the control of the MLD in the seasonal variation of nutrients, with a winter supply of nutrients from intermediate or deep waters when the mixed layer deepens, and low or undetectable nutrients when the MLD is shallow. It can be noticed that the highest nutrient values were detected at ANTARES during the deep convection year 2012-2013 (see Figures 2C, D, G, H of the Supplementary Material), despite being outside the deep convection of the GoL.

4 Identification and filtering of the seasonal variability drivers

4.1 Seawater pCO_2 variability

In the NW Mediterranean Sea, the pCO_2^{IS} seasonal variability is driven by thermal and non-thermal drivers that act in opposition [*e.g.*, Bégovic and Copin-Montégut, 2002; Copin-Montégut et al., 2004; De Carlo et al., 2013; Wimart-Rousseau et al., 2020; Ulses et al., 2022]. Figure 4 presents the respective contributions of thermal (δpCO_2^{TD}) and non-thermal processes (δpCO_2^{N}) on

TABLE 1 Mean values within the mixed layer for different parameters measured at DYFAMED and ANTARES from January 2010 to December 2019.

DYFAMED	Mean ± SD	Min. - Max.	n	ANTARES	Mean ± SD	Min. - Max.	n
Temp. [°C]	16.79 ± 3.42	13.14 - 24.62	100	Temp. [°C]	18.52 ± 4.03	13.17 - 26.64	66
Salinity	38.25 ± 0.11	37.82 - 38.48	100	Salinity	38.20 ± 0.15	37.89 - 38.49	64
A_T [µmol.kg-1]	2571 ± 17	2528 - 2626	98	A_T [µmol.kg-1]	2567 ± 13	2536 - 2596	51
C_T [µmol.kg-1]	2269 ± 27	2224 - 2343	97	C_T [µmol.kg-1]	2258 ± 26	2222 - 2333	51
pH_T^{25}	7.969 ± 0.034	7.912 - 8.037	92	pH_T^{25}	7.982 ± 0.038	7.896 - 8.045	49
pH_T^{IS}	8.093 ± 0.026	8.016 - 8.141	92	pH_T^{IS}	8.083 ± 0.037	7.973 - 8.145	49
pCO_2^{25} [µatm]	542 ± 51	445 - 633	92	pCO_2^{25} [µatm]	522 ± 57	435 - 665	49
pCO_2 [µatm]	386 ± 28	338 - 477	92	pCO_2 [µatm]	397 ± 41	334 - 528	49
NO_3^- [µmol.kg-1]	0.43 ± 0.58	0 - 1.98	86	NO_3^- [µmol.kg-1]	0.47 ± 1.04	0 - 6.27	65
PO_4^{3-}[µmol.kg1]	0.04 ± 0.02	0 - 0.10	83	PO_4^{3-}[µmol.kg1]	0.04 ± 0.04	0 - 0.21	63
NO_2^-[µmol.kg1]	0.04 ± 0.05	0 - 0.18	74	NO_2^-[µmol.kg1]	0.05 ± 0.07	0 - 0.28	65
$SiOH_4$[µmol.kg 1]	1.08 ± 0.48	0 - 1.99	91	$SiOH_4$[µmol.kg 1]	1.87 ± 0.91	0.49 5.46	65
Ω_C	5.17 ± 0.32	4.67 - 5.84	92	Ω_C	5.29 ± 0.36	4.54 - 5.94	49
Ω_A	3.42 ± 0.21	3.09 - 3.87	92	Ω_A	3.50 ± 0.24	3.00 - 3.93	49
MLD [db]	37 ± 26	10 - 85	100	MLD [db]	28 ± 21	10 - 86	66

SD stands for Standard Deviation. Min. and Max. stand for minimum and maximum values measured and n refers to the number of values.

pCO_2^{IS} at DYFAMED (Figure 4A) and ANTARES (Figure 4B). Over the studied period, variations of pCO_2^{IS} (Figures 2I, K of the Supplementary Material) occurred mainly because of changes in surface seawater temperature. Figures 4A, B indicate a regular seasonal pattern for the δpCO_2^{TD} with the highest values in summer and the lowest values in winter and early spring (Table 2). Nonetheless, the pCO_2^{IS} changes observed at both sites were less than those expected from the thermodynamic effect of sea surface temperature variation from 13°C to 26°C (*ca.* 240 µatm).

Changes in seawater pCO_2 induced by non-thermal processes are represented by the δpCO_2^N which is considered to be mainly due to biological activity, but could also include changes due to advection, vertical diffusion, and air-sea gas exchanges [Takahashi et al., 1993]. Seasonal variation is observed at both sites for δpCO_2^N within the mixed layer, from a maximum in winter to a minimum in summer (Figures 4A, B). This indicates that, over an annual cycle, the thermal effects on seawater pCO_2 variability were partially compensated by other processes. Unlike pCO_2, the C_T content is not directly influenced by temperature, meaning that seawater pCO_2 variations that are not due to temperature changes might be related to C_T variations if A_T remains constant [*e.g.*, Takahashi et al., 2002]. Significant relationships between pCO_2^N and C_T

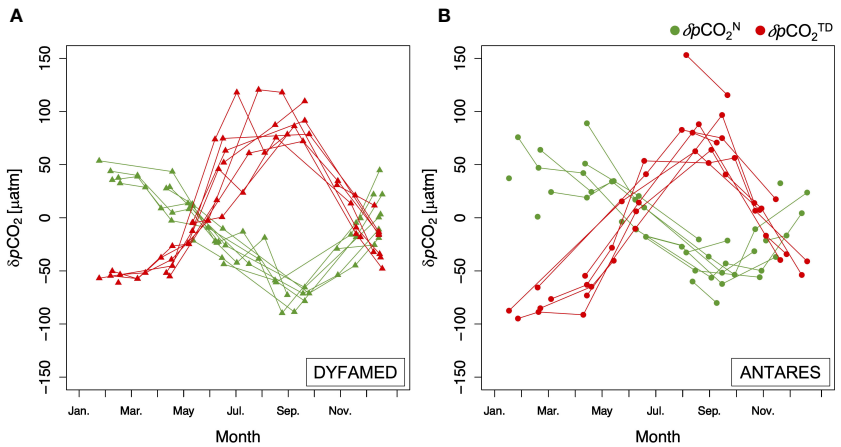

FIGURE 4
Interannual variability in thermal and non-thermal contributions to pCO_2 within the mixed layer at the DYFAMED **(A)** and ANTARES **(B)** sites from January 2010 to December 2019. δpCO_2^{TD}: pCO_2 changes induced by temperature (δpCO_2^{TD} = pCO_2 - pCO_2^N; red lines); δpCO_2^N: pCO_2 changes induced by other processes (δpCO_2^N = pCO_2 - pCO_2^{TD}; green lines). When no data have been acquired during three consecutive months, dots have not been joined.

TABLE 2 Variability of seawater pCO_2 data measured at *in situ* temperature (pCO_2^{IS}), induced by temperature changes (Temp-Driven - pCO_2^{TD}), and induced by to non-thermal effects (pCO_2^{N}) in the mixed layer at the DYFAMED and ANTARES sites.

	DYFAMED		ANTARES	
	Min.-Max. [µatm]	Contribution [%]	Min.-Max. [µatm]	Contribution [%]
pCO_2^{IS}	338-477	/	334-528	/
pCO_2^{TD}	330-536	45-87	318-561	49-79
pCO_2^{N}	316-455	44-63	332-514	41-49

Contributions in terms of percentage have been calculated according to the range of pCO_2^{IS} variability.
"/" stands for "not applicable".

normalised to a constant salinity are observed (n = 47, p-value< 2.2×10^{-16}, r^2 = 0.90 at ANTARES and n = 95, p-value<2.2×10^{-16}, r^2 = 0.82 at DYFAMED). At DYFAMED, Bégovic and Copin-Montégut (2002) demonstrated that these C_T changes are mostly due to biological processes in late winter and spring, and to water mass mixing and air-sea exchanges in autumn and early winter.

4.2 Biological contribution to the seasonal pCO_2 variability

In a given water parcel found in the upper part of the water column, biological processes impact the carbonate system variables and thus the air-sea CO_2 exchanges. To understand the overall impact of these processes on the seasonal changes in A_T and C_T, salinity-normalised changes of A_T and C_T in the mixed layer are plotted in Figure 5A. The system is assumed to be closed (unimpacted by external factors) and theoretical impacts of physical and biological processes driving the variability of A_T and C_T have been added as presented in Zeebe and Wolf-Gladrow (2001). During $CaCO_3$ formation, A_T change is twice as much as C_T as one mole of carbon and one mole of Ca^{2+} are used, leading to a decrease of C_T and A_T in a ratio 1:2. While photosynthesis and respiration tend to decrease and increase the C_T content to produce Redfield organic matter, respectively, both processes have a minor effect on A_T because in addition to inorganic carbon, nutrients are taken up and released by photosynthesis and respiration, respectively [Zeebe and Wolf-Gladrow, 2001]. Finally, air-sea CO_2 exchanges only affect the C_T content as the uncharged CO_2 will not affect the A_T quantity describing the ion-charge balance in the water. In Figure 5A, the mean NA_T and NC_T values during each season have been reported and considered as representative of each season's mean values. Thus, similarities between the two sites concerning their seasonality and their biological contributions are presented in Figure 5A which is relevant for diagnostic purposes rather than for a substantial quantification of biological processes to carbonate system parameter variations.

In this considered closed system, mean salinity-normalised A_T and C_T concentrations presented a seasonal variability with values that seemed to spread along the photosynthesis respiration line at both sites, indicating that primary production and remineralisation could control the carbonate chemistry variability. From spring to autumn (yellow, red, and green dots in Figure 5A), data distribution seems to point towards an autotrophic environment with points moving along the vector representing this process, while dots in winter appear to line up along the respiration vector which could indicate the occurrence of heterotrophic processes (blue dots in Figure 5A). Moreover, it has to be noticed that the MLD shows strong seasonal variations (see Section 3.1.) with a mixed layer deeper than the euphotic zone in winter [Mayot et al., 2017]. In the studied area, Marty and Chiaverini (2002) have calculated primary production estimates using the ^{14}C method and reported new production that ranged from 19 to 71 $gC.m^{-2}.a^{-1}$. Considering the mean mixed layer depth and density values measured at DYFAMED (Table 1), the C_T consumption associated with these new production rates has been calculated. The values deduced lie between 41.6 $\mu mol.kg^{-1}.a^{-1}$ and 155.5 $\mu mol.kg^{-1}.a^{-1}$, which is in good agreement with the observed C_T ranges reported in this study. Whilst several assumptions are made in Figure 5A, the means shift along the year could highlight a link to seasonal biological processes.

In the ocean, the onset of primary production is related to the temperature through its direct impacts on the water column stratification (represented by the MLD) [Sverdrup, 1953]. Moreover, the occurrence of biological processes should lead to systematic inter-property relationships between seasonal changes of nutrients and C_T [Redfield et al., 1963]. Figures 5C, D show variations between salinity-normalised nitrate concentrations ($N.NO_3^-$) and temperature (Figure 5C), and between NC_T and temperature (Figure 5D). Over a year, the concentrations of $N.NO_3^-$ and NC_T were seasonally related to the temperature, with the highest values measured in winter for both parameters and an almost linear decrease with the increasing temperature during the rest of the year for the NC_T content. With regard to biogeochemical processes, data measured within the ML in the studied region are in agreement with the literature: from spring to autumn, and with the stratification of the water column, autotrophic processes lead to a decrease in the C_T content and to the depletion of nutrients, while the winter deepening of the MLD due to the cooling of surface waters supplies inorganic nutrients and C_T in the upper water column [e.g., Bégovic and Copin-Montégut, 2002; Touratier et al., 2016; Ulses et al., 2016; Ulses et al., 2022]. On seasonal timescales, both sites seem to act equally and to be impacted almost similarly by the same processes. In this area, MLD deepening events are the main

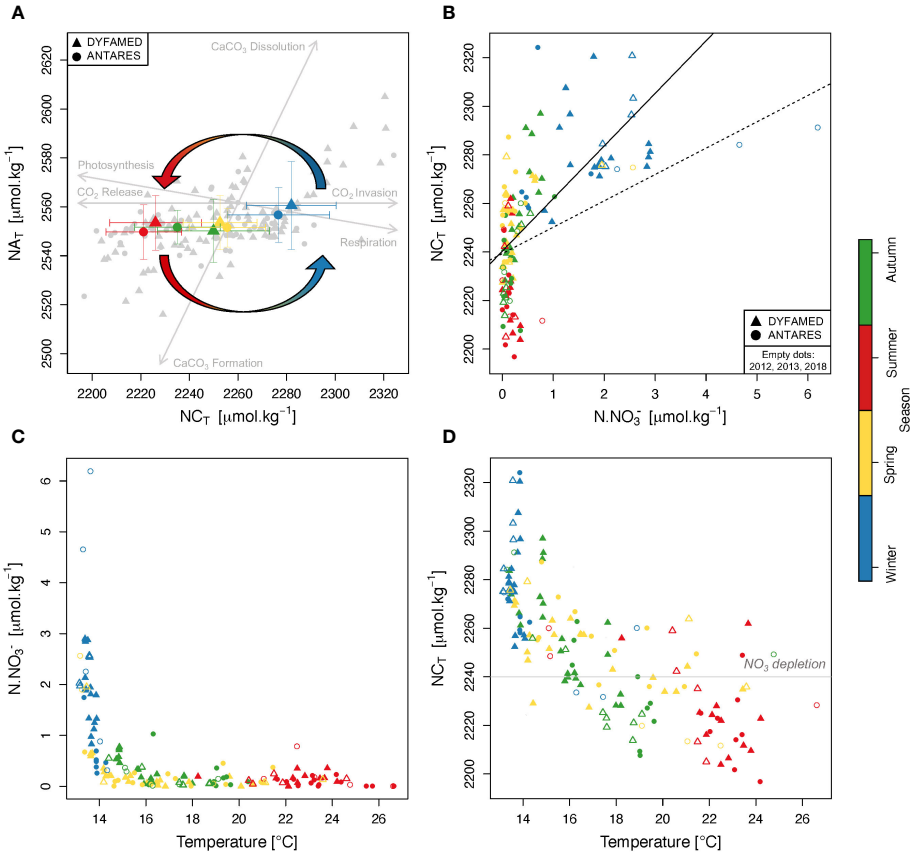

FIGURE 5
(A) Salinity-normalised A_T (NA_T) vs. salinity-normalised C_T (NC_T), **(B)** NC_T vs. salinity-normalised NO_3^- ($N.NO_3^-$), **(C)** $N.NO_3^-$ vs. temperature and **(D)** NC_T vs. temperature within the mixed layer from January 2010 to December 2019 at ANTARES (circle dots) and DYFAMED (triangle dots). On figure **(A)**, grey vectors reflect theoretical impacts of various processes (photosynthesis/respiration, carbonate dissolution/formation, CO_2 release/invasion) on A_T and C_T adapted from Zeebe and Wolf-Gladrow [2001]. On **(B–C)** and **(D)**, empty dots represent data measured during the winter deep-convection years of 2012, 2013 and 2018. On **(B)**, full and dotted lines represent the linear regressions for DYFAMED and ANTARES, respectively. The colour scale corresponds to the season: winter in blue (January – March), spring in yellow (April – June), summer in red (July – September), and autumn in green (October – December).

source of new nitrogen in the photic layer [Copin-Montégut, 2000; Moutin and Raimbault, 2002].

At ANTARES and DYFAMED, regression analyses between NC_T and $N.NO_3^-$ yield almost similar NC_T concentrations of *ca.* 2240 µmol.kg^{-1} at zero-nitrate (Figures 5B, D). In a nutrient-depleted NW Mediterranean Sea, this value represents primarily the effect of CO_2 gas solubility and a lesser effect of $CaCO_3$ dissolution [Zeebe, 2012]. Thus, using the mean temperature, salinity, and alkalinity values at each site, seawater pCO_2 values of 365 µatm and 338 µatm have been calculated at ANTARES and DYFAMED, respectively. Considering a mean atmospheric partial pressure value of 402 µatm [the mean annual pCO_2^{ATM} value recorded between 2010 and 2019 at Lampedusa; Dlugokencky et al. (2021)], these values indicate that, if the area was nutrient depleted, waters within the mixed layer would be undersaturated with respect to the pCO_2^{ATM} and act as a CO_2 sink for the atmosphere. In consequence, the C_T content would increase. Over the year, a depletion in the nutrient content has been observed near the end of spring blooms (Figures 2A–H of the Supplementary Material). Nevertheless, considering that the zero-nitrate condition occurs when the temperature reaches *ca.* 15°C (Figure 5C), decreasing C_T values have been observed when the temperature increases in the absence of nitrate fluxes (Figure 5D). This seasonal C_T variability has been previously reported in the literature [*e.g.*, Copin-Montégut, 2000]. If these nutrient-free waters are warmed to a temperature up to 25°C as it could happen from June onwards in the studied area (Figure 5D), they would become supersaturated with respect to atmospheric CO_2 and the C_T content would decrease. In consequence, the mixed layer C_T loss observed in summer and autumn could be related to physical processes (mixing and advection of water masses) as well as through an outgassing to the atmosphere. Besides biological contribution to C_T changes, this suggests that physical processes play a key role in modulating the C_T content. In addition, the possible occurrence of a more regeneration-dominated system could be suggested to explain the observed C_T content variability [Marty and Chiaverini, 2002].

10.3389/fmars.2023.1281003

5 Long-term temporal changes of the carbonate system within the mixed layer

5.1 Determination of the CO_2 system trends

In the NW Mediterranean Sea, seasonal cycles of carbonate chemistry parameters presented almost similar functioning at ANTARES and DYFAMED. This section will focus on the long-term variability and evaluate whether both sites are analogous in terms of carbonate chemistry changes over ten years.

For the global surface ocean, Lauvset et al. (2015) evaluated contrasting fCO_2 and pH_T trends between 1991 and 2011 with values ranging from +0.23 to +3.51 µatm.a^{-1} for fCO_2, and between -0.0010 and -0.0027 pH unit.a^{-1} for pH_T. Based on seven oceanic long-term time-series analyses, Bates et al. (2014) reported decreasing trends for pH_T varying between -0.0013 and -0.0026 pH unit.a^{-1} and increasing C_T trends ranging between +0.64 and +1.78 µmol.kg^{-1}.a^{-1}. At the DYFAMED site, previous studies reported decreasing trends for the pH in subsurface waters (-0.0022 pH unit.a^{-1} – Merlivat et al. (2018); -0.0030 pH unit.a^{-1} – Marcellin Yao et al. (2016)) and increasing trends for C_T (1.40 ± 0.15 µmol.kg^{-1}.a^{-1} – Merlivat et al. (2018)). By combining different datasets acquired between 1998 and 2016 from coastal and open ocean sites in the Ligurian Sea, Coppola et al. (2020) reported positive surface trends for both C_T and pCO_2 equal to 0.59 ± 0.34 µmol.kg^{-1}.a^{-1} and 3.3 ± 0.7 µatm.a^{-1}, respectively, and a pH annual decrease of -0.0030 ± 0.0010 pH unit (between 0 and 20 meters).

Using the raw datasets at ANTARES and DYFAMED, an increase in C_T within the mixed layer between 2010 and 2019 of +3.8 ± 1.4 µmol.kg^{-1}.a^{-1} at ANTARES and +2.4 ± 1.1 µmol.kg^{-1}.a^{-1} at DYFAMED was estimated (Table 3). Trends were not significant for pCO_2^{IS} and pH^{IS} at DYFAMED. Moreover, no significant trends were observed for either A_T or NA_T at either site. Due to the strong seasonal cycle affecting the C_T content (but also the pCO_2 and pH), the trends reported could be affected by the data distribution along the year. To address this issue, datasets have been "deseasonnalised". This analytical procedure allows the comparison of trends with different increments and lengths [Wanninkhof et al., 2019]. The long-term temporal trends have been calculated using the residual between the harmonic fits and measured values. At both sites, the deseasonnalised datasets were significantly different (t-test according to the significance of the test (p-value) and the degree of freedom (df) obtained) in comparison with the raw datasets for C_T, pCO_2^{IS} and pH^{IS} (Figure 6). Based on the deseasonnalised datasets, significant increases in C_T (+3.2 ± 0.9 µmol.kg^{-1}.a^{-1} – ANTARES; +1.6 ± 0.8 µmol.kg^{-1}.a^{-1} – DYFAMED), seawater pCO_2^{IS} (+5.5 ± 1.8 µatm.a^{-1} – ANTARES; +2.5 ± 1.0 µatm.a^{-1} – DYFAMED) and decreases in pH^{IS} (-0.0045 ± 0.0015 pH unit.a^{-1} – ANTARES; -0.0022 ± 0.0009 pH unit.a^{-1} – DYFAMED) have been measured within the mixed layer between 2010 and 2019 (Figure 6, Table 3). This confirms that the estimation of long-term trends is impacted by the seasonal variability of the environmental parameters, and it supports the deseasonnalisation procedure used in this study to calculate the temporal trends. Nevertheless, trend estimates for DYFAMED are in good agreement with previous estimates at this site [*e.g.*, Merlivat et al., 2018; Coppola et al., 2020], whereas the trends calculated at the ANTARES site are significantly higher than at DYFAMED. Recently, Sutton et al. (2022) proposed new best practices for assessing trends of ocean acidification time-series. For the first time, several trend analysis techniques that have been published in the past have been packaged together into a set of best practices. Through a unique and new 6-step sequence of procedures, a new best practice for assessing and reporting ocean acidification trends as well as variability in ocean carbonate has been proposed. By applying these trend analysis techniques to the ANTARES and DYFAMED datasets, significant decreases in pH^{IS} of -0.0060 ± 0.0012 pH unit.a^{-1} (n=42, p=1.9×10^{-5}) and -0.0018 ± 0.0009 pH unit.a^{-1} (n=58, p=4.6×10^{-2}), respectively, have been obtained. Trends assessed following this procedure are in agreement with the ones derived using the deseasonalised datasets, confirming a higher seawater pH decrease at ANTARES than at DYFAMED.

Due to rough weather conditions, the ANTARES sampling site has experienced more cruise cancellations than DYFAMED. To test the impact of this reduced number of cruises at ANTARES on the calculated temporal trends, the DYFAMED dataset was filtered to follow the same sampling grid than the ANTARES one (Table 3). Considering the resulting C_T trend, the difference between the C_T changes at ANTARES and DYFAMED remains, confirming that

TABLE 3 Estimated annual trend for C_T based on different estimation methods.

		DYFAMED	ANTARES
		Annual C_T changes [µmol.kg^{-1}.a^{-1}]	Annual C_T changes [µmol.kg^{-1}.a^{-1}]
Gross datasets*		+2.4 ± 1.1 (n=58, p=3.4×10^{-2})	+3.8 ± 1.4 (n=42, p=1.1×10^{-2})
Deseasonnalised datasets		+1.6 ± 0.8 (n=58, p=4.6×10^{-2})	+3.2 ± 0.9 (n=42, p=1.2×10^{-3})
ANTARES sampling grid**		+1.8 ± 0.8 (n=36, p=4.2×10^{-2})	/
Removal of the deep water mixing events	Without 2012	+2.8 ± 1.2 (n=55, p=1.5×10^{-2})	+3.2 ± 1.0 (n=40, p=2.1×10^{-3})
	Without 2013	+2.5 ± 1.1 (n=53, p=3.0×10^{-2})	+3.8 ± 0.9 (n=34, p=1.8×10^{-4})
	Without 2018	+3.0 ± 1.0 (n=50, p=4.9×10^{-3})	+2.9 ± 1.0 (n=40, p=4.9×10^{-3})
	Without 2012, 2013 & 2018	+3.7 ± 1.1 (n=42, p=9.2×10^{-4})	+3.5 ± 1.0 (n=30, p=1.3×10^{-3})

*Datasets were significantly different: C_T (t-test=-513.2, df=76.0, p-value<2.2 ×10^{-16} –ANTARES; t-test=-607.8, df= 105.9, p-value<2.2×10^{-16} – DYFAMED), pCO_2^{IS} (t-test = -50.7, df= 73.9, p-value<2.2 ×10^{-16} – ANTARES; t-test = - 75.8, df= 101.3, p-value<2.2 ×10^{-16} – DYFAMED) and pH_T^{IS}(t-test = -1149.1, df= 72.2, p-value<2.2 ×10^{-16} – ANTARES; t-test = -1742.3, df= 100.1, p-value<2.2 ×10^{-16} – DYFAMED).
**The DYFAMED dataset has been filtered to follow the ANTARES sampling grid.
The confidence interval has been added for each calculated trend with the number of values used (n) and the significance of the trend (p-value).
"/" stands for "not applicable".

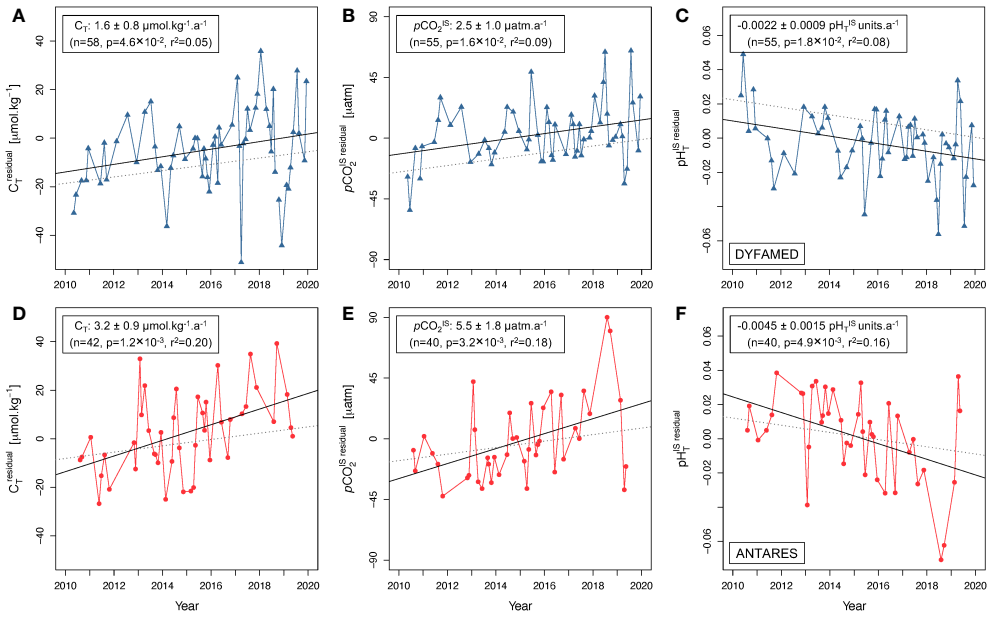

FIGURE 6
Temporal variation at the DYFAMED [blue dots, **(A-C)**] and ANTARES [red dots, **(D-F)**] sites of the residuals of total dissolved inorganic carbon (C_T - µmol.kg^{-1}; a and d), the residuals of partial pressure of CO_2 measured at *in situ* temperature [pCO_2^{IS} - µatm; **(B, E)**] and the residuals of pH measured at *in situ* temperature [pH^{IS}; **(C, F)**] within the mixed layer. Residuals were calculated by subtracting the harmonic fit values from the measured values. Estimated trends are obtained from the slope values of a linear regression between the studied parameters and time. In addition, the estimated annual changes considering air-sea equilibrium have been added for each parameter with the dotted lines. The confidence interval has been added for each trend with the coefficient of determination (r^2), the number of values used (n) and the significance of the trend (p-value).

the difference in trends cannot be attributed to the reduced number of cruises at ANTARES.

The NW Mediterranean Sea encounters major convection events during the winter with a clear deepening of the MLD [*e.g.*, Marty and Chiaverini, 2010; Pasqueron de Fommervault et al., 2015; Merlivat et al., 2018]. In recent years, deep-water mixing events as well as marine heat waves have been reported in the GoL and the Ligurian Sea [*e.g.*, Houpert et al., 2016; Juza et al., 2022]. In this study, we particularly observed MLD deepening in 2012, 2013 and 2018 (see Figure 1 of the Supplementary Material and Section 1). To estimate the impact of these episodes on the long-term trends, temporal changes in C_T have been calculated by removing each of these years (Table 3). At the DYFAMED site, slightly higher trends are reported when each year is removed. At ANTARES, except for the year 2018 which decreases the C_T trend, no significant change can be reported. Thus, particular years of deep-water mixing have marginal impacts on the temporal trends. When removing those peculiar years from long-term trends calculations, the increasing C_T trend is significantly higher at DYFAMED. This could be attributed to the marked injection of nutrients from the deep-water stock into the upper water column that could sustain more primary production and lead to a decrease in the C_T content after the mixing event [Marty and Chiaverini, 2010]. Somehow, this indicates that the carbonate parameters variability is controlled and softened, at the decadal scale, by intense winter mixing [Touratier et al., 2016].

In the coming decades, a weakening of the vertical mixing and dense water formation processes is predicted in the North Western Mediterranean Sea in the context of climate change [*e.g.*, Somot et al., 2006]. In addition, the projected warmer Mediterranean Sea [*e.g*, Nykjaer, 2009] is expected to be more stratified and oligotrophic as a result of the decreasing nutrients supplied by rivers [*e.g.*, Pagès et al., 2020]. In consequence, based on these projections, a reduction in the O_2 supply to the intermediate and deep waters would be observed and the annual C_T variation in surface waters due to primary production processes would be reduced leading to an increase in the C_T content [Reale et al., 2022]. These 10-year time-series highlight that additional measurements will be necessary in time to determine long-term trends while supporting the urgent need for sustained observations from time-series stations to understand the climate change-related consequences the Mediterranean Sea is facing.

5.2 Contribution of anthropogenic CO_2

Between 2010 and 2019, a mean annual increase of 2.41 ± 0.11 µatm.a^{-1} in pCO_2^{ATM} has been recorded at the Lampedusa site [equivalent to the trend recorded at global scale; Dlugokencky et al. (2021)]. To estimate the sensitivity of the calculated trends to the increase in atmospheric CO_2, the increase in pCO_2^{ATM} was assumed to be equivalent to an increase in surface ocean pCO_2 (Figure 6). Considering the mean salinity, temperature, and alkalinity values for each site, if an air-sea equilibrium is assumed, corresponding changes in C_T would be equal to 1.30 µmol.kg^{-1}.a^{-1} at both sites. Considering the trends of C_T measured at both sites, the contribution due to ocean uptake of atmospheric CO_2 over the last 10 years explains most of the C_T increase at DYFAMED, while it accounts for about half of the C_T increase at ANTARES.

The increase in atmospheric pCO_2 during the last 10 years may induce a shift in the status of sink or source for atmospheric CO_2. Cossarini et al. (2021), through a reanalysis of the Mediterranean Sea biogeochemistry that covers the period 1999–2019, reported a slight shift in CO_2 behavior from a source to a sink of atmospheric CO_2 over the last decade in the open sea areas. Estimation of the temporal pCO_2 excess (ΔpCO_2) variability at the ANTARES and DYFAMED sites, represented in Figure 7, shows positive ΔpCO_2 values (a "source" status) in summer and spring and negative values (a "sink" status) in winter and autumn at both sites. It should be noted, however, that rigorous estimates of air-sea fluxes need to take into account wind speed, as they induce modulations in the air-sea gas transfer velocities [Ho et al., 2006]. It is also worth noting that the datasets, by merging measurements acquired during convective events years and low-resolution sampling grids, induce several limitations. Nevertheless, previous estimates based on *in situ* data measured at the DYFAMED site reported the same seasonal pattern for air-sea CO_2 fluxes [*e.g.*, Bégovic and Copin-Montégut, 2002]. At the studied sites, while the pCO_2^{IS} temporal trends reported are higher than the increase in the pCO_2^{ATM} [Dlugokencky et al., 2021], no clear temporal trend was observed for ΔpCO_2 at either site.

This suggests that, over this 10-year period, mechanisms of control seem to counterbalance the increasing atmospheric pCO_2 trend. Nonetheless, it can be noticed that, in the future, higher seawater pCO_2^{IS} values can be expected in response to the warming tendency of the Mediterranean Sea waters [*e.g*, Nykjaer, 2009], with a concomitant increase of the stratification of the water column [*e.g*, Somot et al., 2006] that could lead to significant ΔpCO_2 changes. Water exchanges at the Strait of Gibraltar result in anthropogenic carbon (C_{ANT}) input from the Atlantic towards the Mediterranean Sea [Flecha et al., 2012] as the surface waters in the Atlantic Ocean are enriched in C_{ANT} with respect to the Mediterranean outflow waters. Recently, Flecha et al. (2019) estimated an annual rate of anthropogenic carbon flux across the Strait of Gibraltar of 1.5 ± 0.6 µmol $kg^{-1}.a^{-1}$ between 2005 and 2015. While the C_{ANT} outflow towards the Atlantic should be considered to correctly calculate the C_{ANT} enrichment of the Mediterranean Sea, this C_{ANT} input needs to be considered to explain the C_T increase recorded in the NW Mediterranean Sea. Nevertheless, even if this input of anthropogenic carbon is considered as a potential source to explain the measured temporal trend, a discrepancy between the two sites remains.

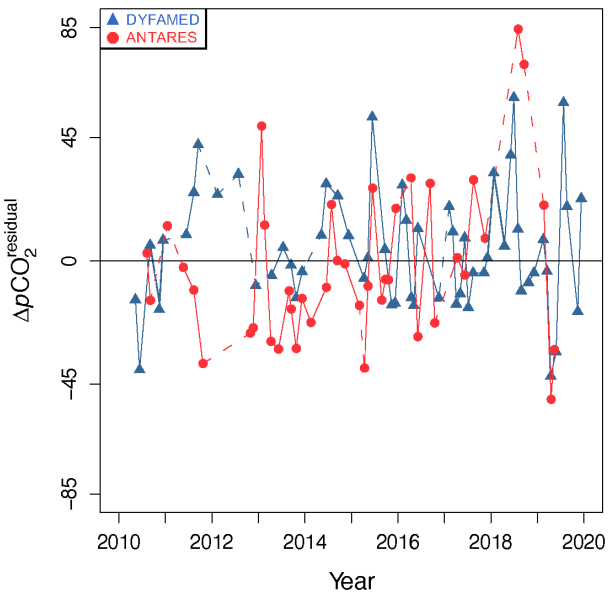

FIGURE 7
Time-series observations of the residuals of the pCO_2 excess calculated as: $\Delta pCO_2 = pCO_2^{IS} - pCO_2^{ATM}$. Residuals have been calculated by subtracting from the measured values the values obtained by harmonic fit. Atmospheric partial pressure of CO_2 recorded at the Lampedusa site from January 2010 to December 2019 [Dlugokencky et al., 2021] were used. A negative ΔpCO_2 indicates potential fluxes directed from the atmosphere to the ocean, and a positive ΔpCO_2 indicates potential fluxes directed from the ocean to the atmosphere. When no data were acquired during three consecutive months, dots were joined by dotted lines.

5.3 Does the Northern Current impact the temporal trends?

Based on several scenarios and trend calculations, and even when considering uncertainties [Millero, 1995; Orr et al., 2018] of the measured (A_T, C_T) and calculated parameters (pCO_2^{IS}, pH), the singularity of the ANTARES site has been highlighted in the previous sections. Nonetheless, the difference between the ANTARES long-term trends and previous estimates, including the DYFAMED time-series, remains to explain. Besides the error associated with these estimates, the ANTARES sampling site location can be considered as a possible explanation. Whereas the DYFAMED site is clearly situated in the open ocean (see Section 3.1.), the ANTARES site is located at the edge of the Ligurian Sea and the GoL, and is located often in the core of the NC (Figure 3) that flows along the continental slope with a seasonal variability and carries fresher AW [Bourg and Molcard, 2021]. In consequence, variability is induced by the path of the NC front that can be sampled at the ANTARES site (Figures 3C, D). The NC structure transports waters with a clear oligotrophic signal [Ross et al., 2016], a fresher signature of Atlantic origin, and also has frontal instabilities that have been associated with a Chl *a* filament signal near the outer boundary [Niewiadomska et al., 2008; Bosse et al., 2021]. By selecting only the data recorded in the inner side of the NC, a higher C_T trend of +5.3 ± 1.8 µmol.$kg^{-1}.a^{-1}$ (n = 16, p-value = 7.7×10^{-3}, r^2 = 0.33) has been recorded. Conversely, a C_T trend of +3.5 ± 1.2 µmol.$kg^{-1}.a^{-1}$ (n = 19, p-value = 7.8×10^{-3}, r^2 = 0.28) is obtained when data in the outside part of the NC are considered. When using a distance criterion varying between 2 and 5 kilometers around or outside the NC core to derive C_T trends, temporal changes vary between +4.1 ± 1.2 µmol.$kg^{-1}.a^{-1}$ (n = 23, p-value = 2.2×10^{-3}, r^2 = 0.31; ± 5 kilometers around the NC core) and +3.6 ± 1.2 µmol.$kg^{-1}.a^{-1}$ (n = 26, p-value = 6.8×10^{-3}, r^2 = 0.22; ± 2 kilometers outside the NC core). Thus, and even if the temporal trends are impacted by the distance criterion selected, C_T trends at ANTARES remain higher than at DYFAMED. This highlights the importance of the sampling location on the estimated trends as coastal environments, or frontal systems associated with the boundary circulation, are more prone to be impacted by biological processes but also land-sea exchanges that could produce regime-

shifts in the local biogeochemistry and modify the alkalinity content. These trend estimates highlight the noticeable impact of the sampling site locations with regard to physical structures to derive long-term temporal changes. Indeed, the NC likely plays a key role in lateral transport along the shore, but also as a barrier across the shore for biogeochemical tracers, with important consequences for the estimated temporal trends in the upper water (between 0 and *ca.* 300 dbars) column where its signal is present [Albérola et al., 1995].

6 Conclusions

Long-term observations of carbonate chemistry at the ANTARES and DYFAMED sites in the NW Mediterranean Sea confirmed previous estimates and showed that the seasonal variability of carbonate parameters is alternatively driven by temperature changes and non-thermal factors, mainly represented by biological processes and vertical exchanges. In addition, this study compares, for the first time, long-term trends acquired in the Ligurian Sea at these two sites. Over the last 10 years, increasing trends in C_T and pCO_2^{IS} and decreasing trends in pH^{IS} have been reported. Nevertheless, the ANTARES long-term observations, which are affected by the NC variability, are higher than those reported elsewhere in the studied area. Since geostrophic currents and mesoscale features are observed throughout the whole NW Mediterranean Sea, this study has reported their influence on the carbonate system parameters and the need to study physical forcings to accurately predict their impact on the carbon cycle. By deciphering seasonal and decadal changes, this study exhibits the duality of the two studied sites: on seasonal timescales, the same factors seem to drive the variability, but on decadal timescales, significant differences are observed between the long-term trends and the two sites are impacted by distinct processes.

In light of the findings of this study, it appears that fixed, long-term time-series are essential, but not sufficient to understand the processes influencing the carbonate system trends. For the future, to get a better insight into the interannual and seasonal variability in the NW Mediterranean Sea, and the specific hydrological conditions observed at ANTARES, further, dedicated studies such as repeated Lagrangian observations of carbonate systems are needed for a better understanding of the processes influencing C_T evolution, and to better constraint the regional evolution of air-sea CO_2 fluxes.

Data availability statement

Publicly available datasets were analyzed in this study. This data can be found here: https://www.seanoe.org/, https://mistrals.sedoo.fr/MOOSE/.

Author contributions

CW-R: Conceptualization, Formal Analysis, Investigation, Validation, Writing – original draft, Writing – review & editing. TW: Conceptualization, Formal Analysis, Investigation, Supervision, Validation, Writing – original draft, Writing – review & editing. AB: Formal Analysis, Visualization, Writing – review & editing. PR: Funding acquisition, Supervision, Validation, Writing – review & editing. LC: Funding acquisition, Resources, Writing – review & editing. MF: Writing – review & editing. CU: Writing – review & editing. DL: Conceptualization, Formal Analysis, Funding acquisition, Investigation, Resources, Supervision, Writing – original draft, Writing – review & editing.

Funding

The author(s) declare financial support was received for the research, authorship, and/or publication of this article. This research paper represents a contribution to the MOOSE program and received support from GROOM-RI project funded by the European Union's Horizon 2020 research and innovation program under grant agreement No 951842.

Acknowledgments

The authors thank the captains and the crews of the N/O Tethys II (French oceanography Fleet, FOF) and the scientific and technical staff involved in sampling the ANTARES and DYFAMED time-series monthly. We acknowledge the MOOSE program and the GROOM-RI project for contributing and supporting this paper. The ANTARES and DYFAMED time-series are funded by the MOOSE program (Mediterranean Ocean Observing System for the Environment) coordinated by CNRS-INSU and the Research Infrastructure ILICO (CNRS-IFREMER). For seawater sample analyses, we also thank the SNAPO-CO2 at LOCEAN, Paris, and in particular J. Fin and N. Metzl. We thank the reviewers for their careful reading of our manuscript and their many insightful comments and suggestions.

Conflict of interest

The authors declare that the research was conducted in the absence of any commercial or financial relationships that could be construed as a potential conflict of interest.

The author(s) declared that they were an editorial board member of Frontiers, at the time of submission. This had no impact on the peer review process and the final decision.

Publisher's note

Supplementary material

The Supplementary Material for this article can be found online at: https://www.frontiersin.org/articles/10.3389/fmars.2023.1281003/full#supplementary-material

References

Albérola, C., Millot, C., and Front, J. (1995). On the seasonal and mesoscale variabilities of the Northern Current during the PRIMO-0 experiment in the western Mediterranean Sea. *Oceanol. Acta* 18 (2), 163–192. doi: 10261/194233

Álvarez, M., Sanleón-Bartolomé, H., Tanhua, T., Mintrop, L., Luchetta, A., Cantoni, C., et al. (2014). The CO_2 system in the Mediterranean Sea: a basin wide perspective. *Ocean Sci.* 10 (1), 69–92. doi: 10.5194/os-10-69-2014

Aminot, A., and Kérouel, R. (2007). *Dosage automatique des nutriments dans les eaux marines: méthodes en flux continu* (Versailles (France): Google-Books-ID: WJa03AhDIGoC. Editions Quae).

Andersen, V., and Prieur, L. (2000). One-month study in the open NW Mediterranean Sea (DYNAPROC experiment, May 1995): overview of the hydrobiogeochemical structures and effects of wind events. *Deep Sea Res. Part I* 47 (3), 397–422. doi: 10.1016/S0967-0637(99)00096-5

Bates, N., Astor, M. Y., Church, M., Currie, K., Dore, J., González-Dávila, M., et al. (2014). A time-series view of changing ocean chemistry due to ocean uptake of anthropogenic CO_2 and ocean acidification. *Oceanography* 27 (1), 126–141. doi: 10.5670/oceanog.2014.16

Bégovic, M., and Copin-Montégut, C. (2002). Processes controlling annual variations in the partial pressure of CO_2 in surface waters of the central northwestern Mediterranean Sea (Dyfamed site). *Deep Sea Res. Part II: Topical Stud. Oceanogr.* 49 (11), 2031–2047. doi: 10.1016/S0967-0645(02)00026-7

Bensoussan, N., and Gattuso, J.-P. (2007). Community primary production and calcification in a NW Mediterranean ecosystem dominated by calcareous macroalgae. *Mar. Ecol. Prog. Ser.* 334, 37–45. doi: 10.3354/meps334037

Berta, M., Bellomo, L., Griffa, A., Magaldi, M., Molcard, A., Mantovani, C., et al. (2018). Wind-induced variability in the Northern Current (northwestern Mediterranean Sea) as depicted by a multi-platform observing system. *Ocean Sci.* 14, 689–710. doi: 10.5194/os-14-689-2018

Birol, F., Cancet, M., and Estournel, C. (2010). Aspects of the seasonal variability of the Northern Current (NW Mediterranean Sea) observed by altimetry. *J. Mar. Syst.* 81 (4), 297–311. doi: 10.1016/j.jmarsys.2010.01.005

Bosse, A., and Fer, I. (2019). Mean structure and seasonality of the norwegian atlantic front current along the mohn ridge from repeated glider transects. *Geophys. Res. Lett.* 46 (22), 13170–13179. doi: 10.1029/2019GL084723

Bosse, A., Testor, P., Damien, P., Estournel, C., Marsaleix, P., Mortier, L., et al. (2021). Wind-forced submesoscale symmetric instability around deep convection in the northwestern mediterranean sea. *Fluids* 6 (3), 123. doi: 10.3390/fluids6030123

Bosse, A., Testor, P., Houpert, L., Damien, P., Prieur, L., Hayes, D., et al. (2016). Scales and dynamics of Submesoscale Coherent Vortices formed by deep convection in the northwestern Mediterranean Sea. *J. Geophys. Res.: Oceans* 121 (10), 7716–7742. doi: 10.1002/2016JC012144

Bourg, N., and Molcard, A. (2021). Northern boundary current variability and mesoscale dynamics: a long-term HF RADAR monitoring in the North-Western Mediterranean Sea. *Ocean Dynam.* 71, 851–870. doi: 10.1007/s10236-021-01466-9

Copin-Montégut, C. (1993). Alkalinity and carbon budgets in the Mediterranean Sea. *Global Biogeochem. Cycles* 7 (4), 915–925. doi: 10.1029/93GB01826

Copin-Montégut, C. (2000). Consumption, production on scales of a few days of inorganic carbon, nitrate, oxygen by the planktonic community. Results of continuous measurements at the Dyfamed station in the northwestern Mediterranean Sea (May 1995). *Deep-Sea Res. Part I* 47 (3), 447–477. doi: 10.1016/S0967-0637(99)00098-9

Copin-Montégut, C., Bégovic, M., and Merlivat, L. (2004). Variability of the partial pressure of CO_2 on diel to annual time scales in the Northwestern Mediterranean Sea. *Mar. Chem.* 85 (3-4), 169–189. doi: 10.1016/j.marchem.2003.10.005

Coppola, L., Boutin, J., Gattuso, J.-P., Lefèvre, D., and Metzl, N. (2020). "The carbonate system in the Ligurian Sea," in *The Mediterranean sea in the era of global change (volume 1),- evidence from 30 years of multidisciplinary study of the Ligurian sea*. Eds. C. Migon, A. Sciandra and P. Nival (London (UK): ISTE Sci. Publ. LTD).

Coppola, L., Diamond Riquier, E., and Carval, T. (2021). doi: 10.17882/43749

Coppola, L., Legendre, L., Lefevre, D., Prieur, L., Taillandier, V., and Diamond Riquier, E. (2018). Seasonal and inter-annual variations of dissolved oxygen in the northwestern Mediterranean Sea. *Prog. Oceanogr.* 162, 187–201. doi: 10.1016/j.pocean.2018.03.001

Coppola, L., Prieur, L., Taupier-Letage, I., Estournel, C., Testor, P., Lefèvre, D., et al. (2017). Observation of oxygen ventilation into deep waters through targeted deployment of multiple Argo-O_2 floats in the north-western Mediterranean Sea in 2013. *J. Geophys. Res.: Oceans* 122 (8), 6325–6341.C. doi: 10.1002/2016JC012594

Coppola, L., Raimbault, P., Mortier, L., and Testor, P. (2019). Monitoring the environment in the northwestern Mediterranean Sea. *Eos* 100. doi: 10.1029/2019EO125951

Cossarini, G., Feudale, L., Teruzzi, A., Bolzon, G., Coidessa, G., Solidoro, C., et al. (2021). High-resolution reanalysis of the mediterranean sea biogeochemistry, (1999–2019). *Front. Mar. Sci.* 8, 741486. doi: 10.3389/fmars.2021.741486

Crépon, M., Wald, L., and Monget, J. M. (1982). Low-frequency waves in the Ligurian Sea during December 1977. *J. Geophys. Res.: Oceans* 87 (C1), 595–600. doi: 10.1029/JC087iC01p00595

Damien, P., Bosse, A., Testor, P., Marsaleix, P., and C. Estournel, C. (2017). Modeling postconvective submesoscale coherent vortices in the northwestern mediterranean sea. *J. Geophys. Res.: Oceans* 122, 9937–9961. doi: 10.1002/2016JC012114

De Carlo, E. H., Mousseau, L., Passafiume, O., Drupp, P. S., and Gattuso, J.-P. (2013). Carbonate chemistry and air–sea CO_2 flux in a NW mediterranean bay over a four-year period: 2007–2011. *Aquat. Geochem.* 19 (5-6), 399–442. doi: 10.1007/s10498-013-9217-4

Dickson, A. G. (1990). Standard potential of the reaction: AgCl(s) +1/2H2(g) = Ag(s) + HCl(aq), and and the standard acidity constant of the ion HSO4- in synthetic sea water from 273.15 to 318.15 K. *J. Mar. Chem.* 15, 113–127. doi: 10.1016/0021-9614(90)90074-Z

Dickson, A. G., and Goyet, C. (1994). *Handbook of methods for the analysis of the various parameters of the carbon dioxide system in sea water. ORNL/CDIAC-74 (Ed.) Version 2, no 74* (Washington, DC: US Department of Energy).

Dickson, A. G., and Millero, F. (1987). A comparison of the equilibrium constants for the dissociation of carbonic acid in seawater media. *Deep Sea Res.* 34 (10), 1733–1743. doi: 10.1016/0198-0149(87)90021-5

Dickson, A. G., and Riley, J. P. (1979). The estimation of acid dissociation constants in seawater media from potentiometric titrations with strong base, I. *ionic product Water – KW. Mar. Chem.* 7, 89–99. doi: 10.1016/0304-4203(79)90001-X

Dickson, A. G., Sabine, C. L., and Christian, J. R. (2007). *Guide to best practices for ocean CO_2 measurements* Vol. 191 (Sidney, BC: PICES special publication. IOCCP report No.8). North Pacific Marine Science Organization.

Dlugokencky, E., Mund, J., Crotwell, A., Crotwell, M., and Thoning, K. (2021). *Atmospheric Carbon Dioxide Dry Air Mole Fractions from the NOAA GML Carbon Cycle Cooperative Global Air Sampling Network. 1968-2019, Version: 2021-02.*

Doney, S., Fabry, V. J., Feely, R., and Kleypas, J. A. (2009). Ocean acidification: the other CO_2 problem. *Annu. Rev. Mar. Sci.* 1 (1), 169–192. doi: 10.1146/annurev.marine.010908.163834

D'Ortenzio, F., Antoine, D., and Marullo, S. (2008). Satellite-driven modelling of the upper ocean mixed layer and air-sea CO_2 flux in the Mediterranean Sea. *Deep Sea Res. Part I* 55, 405–434. doi: 10.1016/j.dsr.2007.12.008

D'Ortenzio, F., Iudicone, D., de Boyer Montegut, C., Testor, P., Antoine, D., Marullo, S., et al. (2005). Seasonal variability of the mixed layer depth in the Mediterranean Sea as derived from in *situ* profiles. *Geophys. Res. Lett.* 32 (12), 1–4. doi: 10.1029/2005GL022463

D'Ortenzio, F., and Ribera d'Alcalà, M. (2009). On the trophic regimes of the Mediterranean Sea: a satellite analysis. *Biogeosciences* 6, 139–148. doi: 10.5194/bg-6-139-2009

Durrieu de Madron, X., Guieu, C., Sempéré, R., Conan, P., Cossa, D., D'Ortenzio, F., et al. (2011). Marine ecosystems' responses to climatic and anthropogenic forcings in the Mediterranean. *Prog. Oceanogr.* 91 (2), 97–166. doi: 10.1016/j.pocean.2011.02.003

Edmond, J. M. (1970). High precision determination of titration alkalinity and total carbon dioxide content of sea water by potentiometric titration. *Deep Sea Res. Oceanogr. Abstracts* 17 (4), 737–750. doi: 10.1016/0011-7471(70)90038-0

Feely, R., Sabine, C., Lee, K., Berelson, W., Kleypas, J., Fabry, V., et al. (2004). Impact of anthropogenic CO_2 on the $caCO_3$ system in the oceans. *Science* 305 (5682), 362–366. doi: 10.1126/science.1097329

Flecha, S., Pérez, F., Murata, A., Makaoui, A., and Huertas, I. (2019). Decadal acidification in Atlantic and mediterranean water masses exchanging at the strait of Gibraltar. *Sci. Rep.* 9, 1-11. doi: 10.1038/s41598-019-52084-x

Flecha, S., Pérez, F., Navarro, G., Ruiz, J., Olivé, I., Rodríguez-Gálvez, S., et al. (2012). Anthropogenic carbon inventory in the Gulf of Cádiz. *J. Mar. Syst.* 92 (1), 67–75. doi: 10.1016/j.jmarsys.2011.10.010

Fourrier, M., Coppola, L., D'Ortenzio, F., Mignon, C., and Gattuso, J.-P. (2022). Impact of intermittent convection in the northwestern Mediterranean Sea on oxygen content, nutrients, and the carbonate system. *J. Geophys. Res.: Oceans* 127, e2022JC018615. doi: 10.1029/2022JC018615

Friedlingstein, P., O'Sullivan, M., Jones, M. W., Andrew, R. M., Gregor, L., Hauck, J., et al. (2022). Global carbon budget 2022. *Earth Sys. Sci. Data* 14, 4811–4900. doi: 10.5194/essd-14-4811-2022

Gruber, N., Bakker, D. C. E., DeVries, T., Gregor, L., Hauck, J., Landschützer, P., et al. (2023). Trends and variability in the ocean carbon sink. *Nat. Rev. Earth Environ.* 4, 119–134. doi: 10.1038/s43017-022-00381-x

Gruber, N., Keeling, C., and Stocker, T. (1998). Carbon-13 constraints on the seasonal inorganic carbon budget at the BATS site in the northwestern Sargasso Sea. *Deep Sea Res. Part I: Oceanogr. Res. Papers* 45 (4-5), 673–717. doi: 10.1016/S0967-0637(97)00098-8

Hassoun, A., Gemayel, E., Krasakopoulou, E., Goyet, C., Abboud-Abi Saab, M., Guglielmi, V., et al. (2015). Acidification of the Mediterranean Sea from anthropogenic carbon penetration. *Deep Sea Res. Part I: Oceanogr. Res. Papers* 102, 1–15. doi: 10.1016/j.dsr.2015.04.005

Herbaut, C., Martel, F., and Crépon, M. (1997). A sensitivity study of the general circulation of the Western Mediterranean Sea. *J. Phys. Oceanogr.* 27 (10), 2126–2145. doi: 10.1175/1520-0485(1997)027<2126:ASSOTG>2.0.CO;2

Ho, D. T., Law, C. S., Smith, M. J., Schlosser, P., Harvey, M., and Hill, P. (2006). Measurements of air-sea gas exchange at high wind speeds in the Southern Ocean: Implications for global parameterizations. *Geophys. Res. Lett.* 33, (16). doi: 10.1029/2006GL026817

Hood, E. M., and Merlivat, L. (2001). Annual to interannual variations of fCO_2 in the northwestern Mediterranean Sea: Results from hourly measurements made by CARIOCA buoys 1995-1997. *J. Mar. Res.* 59 (1), 113–131. doi: 10.1357/002224001321237399

Houpert, L., Durrieu de Madron, X., Testor, P., Bosse, A., D'Ortenzio, F., Bouin, M. N., et al. (2016). Observations of open-ocean deep convection in the northwestern Mediterranean Sea: Seasonal and interannual variability of mixing and deep water masses for the 2007-2013 Period. *J. Geophys. Res.: Oceans* 121 (11), 8139–8171. doi: 10.1002/2016JC011857

IPCC (2021). *Climate Change 2021: The Physical Science Basis. Contribution of Working Group I to the Sixth Assessment Report of the Intergovernmental Panel on Climate Change*. Eds. V. Masson-Delmotte, P. Zhai, A. Pirani, S. L. Connors, C. Péan, S. Berger, N. Caud, Y. Chen, L. Goldfarb, M. I. Gomis, M. Huang, K. Leitzell, E. Lonnoy, J. B. R. Matthews, T. K. Maycock, T. Waterfield, O. Yelekçi, R. Yu and B. Zhou (Cambridge, United Kingdom and New York, NY, USA: Cambridge University Press).

Juza, M., Fernández-Mora, À., and Tintoré, J. (2022). Sub-regional marine heat waves in the mediterranean sea from observations: long-term surface changes, sub-surface and coastal responses. *Front. Mar. Sci.* 9, 785771. doi: 10.3389/fmars.2022.785771

Kapsenberg, L., Alliouane, S., Gazeau, F., Mousseau, L., and Gattuso, J.-P. (2017). Coastal ocean acidification and increasing total alkalinity in the northwestern Mediterranean Sea. *Ocean Sci.* 13, 411–426. doi: 10.5194/os-13-411-2017

Kroeker, K. J., Kordas, R. L., Crim, R., Hendriks, I. E., Ramajo, L., Singh, G. S., et al. (2013). Impacts of ocean acidification on marine organisms: quantifying sensitivities and interaction with warming. *Global Change Biol.* 19 (6), 1884–1896. doi: 10.1111/gcb.12179

Lauvset, S. K., Gruber, N., Landschützer, P., Olsen, A., and Tjiputra, J. (2015). Trends, drivers in global surface ocean pH over the past 3 decades. *Biogeosciences* 12, 1285–1298. doi: 10.5194/bg-12-1285-2015

Leblanc, K., Queguiner, B., Diaz, F., Cornet, V., Michel-Rodriguez, M., Durrieu de Madron, X., et al. (2018). Nanoplanktonic diatoms are globally overlooked but play a role in spring blooms and carbon export. *Nat. Commun.* 9 (1), 953. doi: 10.1038/s41467-018-03376-9

Lee, K., Sabine, C. L., Tanhua, T., Kim, T.-W., Feely, R. A., and Kim, H.-C. (2011). Roles of marginal seas in absorbing and storing fossil fuel CO_2. *Energy Environ. Sci.* 4 (19), 1133–1146. doi: 10.1039/c0ee00663g

Lefèvre, D. (2010). *MOOSE (ANTARES)*. doi: 10.18142/233

Louanchi, F., Boudjakdji, M., and Nacef, L. (2009). Decadal changes in surface carbon dioxide and related variables in the Mediterranean Sea as inferred from a coupled data-diagnostic model approach. *ICES J. Mar. Sci.* 66 (7), 1538–1546. doi: 10.1093/icesjms/fsp049

Marcellin Yao, K., Marcou, O., Goyet, C., Guglielmi, V., Touratier, F., and Savy, J.-P. (2016). Time variability of the north-western Mediterranean Sea pH over 1995–2011. *Mar. Environ. Res.* 116, 51–60. doi: 10.1016/j.marenvres.2016.02.016

Margirier, F., Testor, P., Heslop, E., Mallil, K., Bosse, A., Houpert, L., et al. (2020). Abrupt warming, salinification of intermediate waters interplays with decline of deep convection in the Northwestern Mediterranean Sea. *Sci. Rep.* 10 (1), 20923. doi: 10.1038/s41598-020-77859-5

Marshall, J., and Schott, F. (1999). Open-ocean convection: Observations, theory, and models. *Rev. Geophys.* 37, 1–64. doi: 10.1029/98RG02739

Marty, J.-C., and Chiaverini, J. (2002). Seasonal and interannual variations in phytoplankton production at DYFAMED time-series station, northwestern Mediterranean Sea. *Deep Sea Reas. Part II* 49, 2017–2030. doi: 10.1016/S0967-0645(02)00025-5

Marty, J.-C., and Chiaverini, J. (2010). Hydrological changes in the Ligurian Sea (NW Mediterranean, DYFAMED site) during 1995-2007 and biogeochemical consequences. *Biogeosciences* 7, 2117–2128. doi: 10.5194/bg-7-2117-2010

Marty, J.-C., Chiaverini, J., Pizay, M. D., and Avril, B. (2002). Seasonal, interannual dynamics of nutrients, phytoplankton pigments in the western Mediterranean Sea at the DYFAMED timeseries station, (1991–1999). *Deep-Sea Res. II* 49, 1965–1985. doi: 10.1016/S0967-0645(02)00022-X

Mayot, N., d'Ortenzio, F., Taillandier, V., Prieur, L., De Fommervault, O. P., Claustre, H., et al. (2017). Physical and biogeochemical controls of the phytoplankton blooms in North Western Mediterranean Sea: A multiplatform approach over a complete annual cycle, (2012–2013 DEWEX experiment). *J. Geophys. Res.: Oceans* 122 (12), 9999–10019. doi: 10.1002/2016JC012052

Mehrbach, C., Culberson, C. H., Hawley, J. E., and Pytkowicz, R. M. (1973). Measurement of the apparent dissociation constants of carbonic acid in seawater at atmospheric pressure. *Limnol. Oceanogr.* 18 (6), 897–907. doi: 10.4319/lo.1973.18.6.0897

Merlivat, L., Boutin, J., Antoine, D., Beaumont, L., Golbol, M., and Vellucci, V. (2018). Increase of dissolved inorganic carbon and decrease in pH in near-surface waters in the Mediterranean Sea during the past two decades. *Biogeosciences* 15 (18), 5653–5662. doi: 10.5194/bg-15-5653-2018

Millero, F. (1995). Thermodynamics of the carbon dioxide system in the oceans. *Geochimica Cosmochimica Acta* 59 (4), 661–677. doi: 10.1016/0016-7037(94)00354-O

Millot, C. (1991). Mesoscale and seasonal variabilities of the circulation in the western Mediterranean. *Dynam. Atmos. Oceans* 15 (3-5), 179–214. doi: 10.1016/0377-0265(91)90020-G

Millot, C. (1999). Circulation in the western mediterranean sea. *J. Mar. Syst.* 20 (1-4), 423–442. doi: 10.1016/S0924-7963(98)00078-5

Moutin, T., and Raimbault, P. (2002). Primary production, carbon export and nutrients availability in western and eastern Mediterranean Sea in early summer 1996 (MINOS cruise). *J. Mar. Syst.* 33-34 (1), 273–288. doi: 10.1016/S0924-7963(02)00062-3

Niewiadomska, K., Claustre, H., Prieur, L., and d'Ortenzio, F. (2008). Submesoscale physicalbiogeochemical coupling across the Ligurian current (northwestern Mediterranean) using a biooptical glider. *Limnol. Oceanogr.* 53 (3), 2210–2225. doi: 10.4319/lo.2008.53.5_part_2.2210

Nykjaer, L. (2009). Mediterranean Sea surface warming 1985–2006. *Climate Res.* 39, 11–17. doi: 10.3354/cr00794

Orr, J., Epitalon, J.-M., Dickson, A. G., and Gattuso, J.-P. (2018). Routine uncertainty propagation for the marine carbon dioxide system. *Mar. Chem.* 207, 84–107. doi: 10.1016/j.marchem.2018.10.006

Pagès, R., Baklouti, M., Barrier, N., Richon, C., Dutay, J.-C., and Moutin, T. (2020). Projected effects of climate-induced changes in hydrodynamics on the biogeochemistry of the mediterranean sea under the RCP 8.5 regional climate scenario. *Front. Mar. Sci.* 7, 957. doi: 10.3389/fmars.2020.563615

Palmiéri, J., Orr, J., Dutay, J.-C., Béranger, K., Schneider, A., Beuvier, J., et al. (2015). Simulated anthropogenic CO_2; storage and acidification of the Mediterranean Sea. *Biogeosciences* 12 (3), 781–802. doi: 10.5194/bg-12-781-2015

Pasqueron de Fommervault, O., Migon, C., D'Ortenzio, F., Ribera d'Alcalà, M., and Coppola, L. (2015). Temporal variability of nutrient concentrations in the northwestern Mediterranean Sea (DYFAMED time-series station). *Deep-Sea Res. Part I* 100, 1–12. doi: 10.1016/j.dsr.2015.02.006

Petrenko, A. A. (2003). Variability of circulation features in the Gulf of Lion NW Mediterranean Sea. *Import. inertial currents. Oceanol. Acta* 26 (4), 323–338. doi: 10.1016/S0399-1784(03)00038-0

Prieur, L., D'Ortenzio, F., Taillandier, V., and Testor, P. (2020). "Physical oceanography of the Ligurian sea," in *the Mediterranean sea in the era of global change (volume 1),- evidence from 30 years of multidisciplinary study of the Ligurian sea*. Eds. C. Migon, A. Sciandra and P. Nival (London (UK): ISTE Sci. Publ. LTD).

Reale, M., Cossarini, G., Lazzari, P., Lovato, T., Bolzon, G., Masina, S., et al. (2022). Acidification, deoxygenation, and nutrient and biomass declines in a warming Mediterranean Sea. *Biogeosciences* 19, 4035–4065. doi: 10.5194/bg-19-4035-2022

Redfield, A., Ketchum, B., and Richards, F. (1963). "The influence of organisms on the composition of sea-water," in *The sea, Vol 2*. Ed. M. N. Hill (New-York (USA): Wiley), 26–77.

Rivaro, P., Messa, R., Massolo, S., and Frache, R. (2010). Distributions of carbonate properties along the water column in the Mediterranean Sea: Spatial and temporal variations. *Mar. Chem.* 121, 236–245. doi: 10.1016/j.marchem.2010.05.003

Ross, O., Fraysse, M., Pinazo, C., and Pairaud, I. (2016). Impact of an intrusion by the Northern Current on the biogeochemistry in the eastern Gulf of Lion, NW Mediterranean. *Estuarine Coastal Shelf Sci.* 170, 1–9. doi: 10.1016/j.ecss.2015.12.022

Schneider, A., Wallace, D. W. R., and Körtzinger, A. (2010). High anthropogenic carbon content in the eastern Mediterranean. *J. Geophys. Res.* 115 (C12), 1-11. doi: 10.1029/2010JC006171

Sokal, R. R., and Rohlf, F. J. (1969). *Biometry. the principles and practices of statistics in biological research. 2nd edn* (San Francisco, CA: W.H. Freeman).

Somot, S., Sevault, F., and Déqué, M. (2006). Transient climate change scenario simulation of the mediterranean sea for the twenty-first century using a high-resolution ocean circulation model. *Climate Dynam.* 27, 851–879. doi: 10.1007/s00382-006-0167-z

Sutton, A. J., Battisti, R., Carter, B., Evans, W., Newton, J., Alin, S., et al. (2022). Advancing best practices for assessing trends of ocean acidification time series. *Front. Mar. Sci.* 9, 1045667. doi: 10.3389/fmars.2022.1045667

Sverdrup, H. U. (1953). On conditions for the vernal blooming of phytoplankton. *ICES J. Mar. Sci.* 18 (3), 287–295. doi: 10.1093/icesjms/18.3.287

Takahashi, T., Olafsson, J., Goddard, J. G., Chipman, D. W., and Sutherland, S. C. (1993). Seasonal variation of $CO_{2\ and}$ nutrients in the high-latitude surface oceans: A comparative study. *Global Biogeochem. Cycles* 7 (4), 843–878. doi: 10.1029/93GB02263

Takahashi, T., Sutherland, S. C., Sweeney, C., Poisson, A., Metzl, N., Tilbrook, B., et al. (2002). Global sea–air CO_2 flux based on climatological surface ocean pCO_2, and seasonal biological and temperature effects. *Deep Sea Res. Part II: Topical Stud. Oceanogr.* 49 (9-10), 1601–1622. doi: 10.1016/S0967-0645(02)00003-6

Tanhua, T., Orr, J. C., Lorenzoni, L., and Hansson, L. (2015). Monitoring of ocean carbon and ocean acidification. *WMO Bull.* 64, (1).

Testor, P., Bosse, A., Houpert, L., Margirier, F., Mortier, L., Legoff, H., et al. (2018). Multi-scale observations of deep convection in the northwestern mediterranean sea during winter 2012-2013 using multiple platforms. *J. Geophys. Res.: Oceans* 123 (3), 1745–1776. doi: 10.1002/2016JC012671

Testor, P., de Young, B., Rudnick, D. L., Glenn, S., Hayes, D., Lee, C. M., et al. (2019). Oceangliders: a component of the integrated goos. *Front. Mar. Sci.* 6, 422. doi: 10.3389/fmars.2019.00422

Testor, P., and Gascard, J.-C. (2006). Post-convection spreading phase in the Northwestern Mediterranean Sea. *Deep Sea Res. Part I* 53 (3), 869–893. doi: 10.1016/j.dsr.2006.02.004

Testor, P., Mortier, L., Coppola, L., Claustre, H., D'Ortenzio, F., Bourrin, F., et al. (2017). *Glider MOOSE sections* (SEANOE). doi: 10.17882/52027

Todd, R., Owens, W., and Rudnick, D. (2016). Potential vorticity structure in the north atlantic western boundary current from underwater glider observations. *J. Phys. Oceanogr.* 46 (1), 327–348. doi: 10.1175/JPO-D-15-0112.1

Touratier, F., and Goyet, C. (2011). Impact of the eastern mediterranean transient on the distribution of anthropogenic CO_2 and first estimate of acidification for the mediterranean sea. *Deep Sea Res. Part I: Oceanogr. Res. Papers* 58 (1), 1–15. doi: 10.1016/j.dsr.2010.10.002

Touratier, F., Goyet, C., Houpert, L., De Madron, X. D., Lefèvre, D., Stabholz, M., et al. (2016). Role of deep convection on anthropogenic CO_2 sequestration in the Gulf of Lions (northwestern Mediterranean Sea). *Deep Sea Res. Part I: Oceanogr. Res. Papers* 113, 33–48. doi: 10.1016/j.dsr.2016.04.003

Ulses, C., Auger, P.-A., Soetaert, K., Marsaleix, P., Diaz, F., Coppola, L., et al. (2016). Budget of organic carbon in the North-Western Mediterranean open sea over the period 2004–2008 using 3-D coupled physical-biogeochemical modeling. *J. Geophys. Res. Oceans* 121, 7026–7055. doi: 10.1002/2016JC011818

Ulses, C., Estournel, C., Marsaleix, P., Soetaert, K., Fourrier, M., Coppola, L., et al. (2022). *Seasonal dynamics and annual budget of dissolved inorganic carbon in the northwestern Mediterranean deep convection region* (Biogeosciences Discussions). doi: 10.5194/bg-2022-219

Uppström, L. R. (1974). The boron/chlorinity ratio of deep-sea water from the Pacific Ocean. *Deep Sea Res.* 21, 161–162. doi: 10.1016/0011-7471(74)90074-6

Van Haren, H., Taupier Letage, I., Aguilar, J., Albert, A., Anton, G., Anvar, S., et al. (2011). Acoustic and optical variations during rapid downward motion episodes in the deep north-western Mediterranean Sea. *Deep Sea Res. Part I: Oceanogr. Res. Papers* 58, 875–884. doi: 10.1016/j.dsr.2011.06.006

van Heuven, S., Pierrot, D., Rae, J., Lewis, E., and Wallace, D. W. R. (2011). *Co2sys v 1.1, matlab program developed for CO_2 system calculations* (ORNL/CDIAC-105b. Oak Ridge, TN: Oak Ridge National Laboratory).

Wanninkhof, R., Triñanes, J., Park, G.-H., Gledhill, D., and Olsen, A. (2019). Large decadal changes in air-sea CO_2 fluxes in the Caribbean sea. *J. Geophys. Res.: Oceans* 124, 6960–6982. doi: 10.1029/2019JC015366

Wimart-Rousseau, C., Lajaunie-Salla, K., Marrec, P., Wagener, T., Raimbault, P., Lagadec, V., et al. (2020). Temporal variability of the carbonate system and air-sea CO_2 exchanges in a mediterranean human-impacted coastal site. *Estuarine Coast. Shelf Sci.* 236, 106641. doi: 10.1016/j.ecss.2020.106641

Zeebe, R. E. (2012). History of seawater carbonate chemistry, atmospheric CO_2, and ocean acidification. *Annu. Rev. Earth Planet. Sci.* 40, 141–165. doi: 10.1146/annurev-earth-042711-105521

Zeebe, R. E., and Wolf-Gladrow, D. A. (2001). *CO_2 in seawater: equilibrium, kinetics, isotopes* Vol. 65 (Amsterdam: Elsevier Oceanography Book Series). 346 pp.

Zoubir, A., and Iskander, D. (2007). *Bootstrap methods and applications* Vol. 24 (Signal Processing Magazine, IEEE), 10–19.